

$t - U - W$ Model of a $d_{x^2-y^2}$ Superconductor in the Proximity of an AF Mott Insulator: Diagrammatic Studies vs. QMC Simulations

T. Eckl, E. Arrigoni and W. Hanke

Institut für Theoretische Physik, Universität Würzburg, Am Hubland, D-97074 Würzburg, Germany

F. F. Assaad

Institut für Theoretische Physik, Universität Stuttgart, Pfaffenwaldring 57, D-70550 Stuttgart, Germany

(May 19, 2019)

We examine the competition and relationship between an antiferromagnetic (AF) Mott insulating state and a $d_{x^2-y^2}$ superconducting (SC) state in two dimensions using semi-analytical, i. e. diagrammatic calculations of the $t - U - W$ model. The AF Mott insulator is described by the ground state of the half-filled Hubbard model on a square lattice with on-site Coulomb repulsion U and nearest neighbor single-particle hopping t . To this model, an extra term W is added, which depends upon the square of the single-particle nearest-neighbor hopping. Staying at half-band filling and a constant value of U , it was previously shown with Quantum-Monte-Carlo (QMC) simulations that one can generate a quantum transition as a function of the coupling strength, W , between an AF Mott insulating state and a $d_{x^2-y^2}$ SC state. Here we complement these earlier QMC simulations with physically more transparent diagrammatic calculations. We start with a standard Hartree-Fock (HF) calculation to capture the “high-energy” physics of the $t - U - W$ model. Then, we derive and solve the Bethe-Salpeter equation, i. e. we account for fluctuation effects within the time-dependent HF or generalized RPA scheme. Spin- and charge-susceptibility as well as the effective interaction vertex are calculated and systematically compared with QMC data. Finally, the corresponding BCS gap equation obtained for this effective interaction is solved.

I. INTRODUCTION

One salient aspect of the high- T_c materials is the vicinity of two, at first sight rather different, states of matter, superconductivity (SC) and antiferromagnetism (AF) in their phase diagram. The transition between the undoped (AF) system at half-filling and the SC phase is driven by doping with mobile holes. In most of the materials, this transition is not direct, and a disordered “spin-glass” phase occurs in between. However, it has been argued that the “clean” material would display a direct transition from AF to SC phases, and that the spin-glass phase occurs due to the high sensitivity to impurity disorder in the vicinity of the phase transition.

A direct transition from an insulating into a SC phase in a quasi-two-dimensional system (such as the high- T_c materials) is a very interesting, yet insufficiently understood issue. In fact, it is not clear whether this transition is second order down to zero temperature, and thus is related to a quantum critical point, or whether there is a finite-temperature classical bicritical point. In the framework of the projected SO(5)-theory of high- T_c superconductivity¹, it has been suggested that the AF and the SC phases may indeed coexist in some portion of the temperature versus doping phase diagram. Another open question is the nature, i. e. the universality class of this transition. For example, it has been suggested that this transition may be controlled by an SO(5)-symmetric fixed point². SO(5) symmetry is thus restored in the long-wavelength limit³, and AF and SC can be described in terms of a unique superspin vector⁴ in the vicinity of the critical point.

Many efforts have been directed towards studying the AF-SC transition in strongly correlated lattice models by numerical techniques such as Quantum-Monte-Carlo (QMC) simulations. As a relevant model, the Hubbard model, is widely accepted for the description of salient features of high- T_c materials. Unfortunately, it is quite difficult to study large enough Hubbard-model systems by QMC, due to the occurrence of the minus-sign problem at finite doping. The numerical problem can, in principle, be cured, if one can drive the AF-SC transition by means of a parameter, alternative to the doping, which conserves particle-hole symmetry and, therefore, avoids the tedious minus-sign problem. This idea was followed through by Assaad, Imada, and Scalapino (AIS)⁶ in terms of their so-called $t - U - W$ model. It rests on adding an interaction term W , which depends

on the square of the nearest-neighbor hopping. This W term can be obtained from a Su-Schrieffer-Heeger type of electron-phonon interaction in the antiadiabatic limit⁵. In QMC simulations^{6–10} this $t - U - W$ model exhibits a transition from an antiferromagnet to a d-wave superconductor at half-filling and at a critical value of the interaction $W_c \approx 0.3t$ ($U = 4t$, $T = 0K$). The QMC data of AIS supports the picture of a continuous quantum phase transition in the sense that the magnetization vanishes continuously at the critical point. The disadvantage of the $t - U - W$ model is that the bandwidth grows substantially with W . Therefore, one of us¹¹ suggested to introduce a phase factor in the W -term which has a d-wave like symmetry. Although this latter model solves the problem of the bandwidth, the existence of a phase transition to a d-wave superconductor remains open.

While QMC calculations provide an essentially exact description of the properties of the model, semi-analytical, i. e. diagrammatic, calculations allow for a more direct understanding of the processes which are responsible for a given phenomenon. For this reason in this paper, we carry out a systematic diagrammatic study of the $t - U - W$ model.

We first consider in Sec. III the simple Hartree-Fock level, which, due to the complexity of the interaction terms, allows for different broken symmetry phases. However, a careful comparison of the energies of these phases shows that the antiferromagnetic phase is always the stablest one, even for very large values of W . This holds for both versions of the $t - U - W$ model which are considered, i. e. with and without phase factors. Moreover, the only allowed superconducting solution in the simple $t - U - W$ model has an *s*-wave symmetry, while *d*-wave symmetry is not allowed. These mean-field results are in strong contrast with the QMC calculations, which predict a transition to a *d*-wave SC state at some finite W ⁶. On the other hand, in the AF region our mean-field results are in very good accord with QMC, in particular concerning single-particle dispersions, as shown in Sec. III.

The relevant transition to the d-wave SC state is dominantly driven by an effective attractive interaction mediated by spin fluctuation, as is the case for the Hubbard model¹². For this reason, one has to consider the effect of spin fluctuations beyond the Hartree-Fock level, in order to reach the SC state. This is done in Sec. IV, where we carry out a complete RPA summation of all particle-hole diagrams (both bubbles and ladders), with Hartree-Fock Green's functions, in order to obtain the frequency- and momentum-dependent spin and charge susceptibility. The solution of the corresponding Bethe-Salpeter equation is technically quite difficult to achieve and significantly more demanding than the standard case of the simple Hubbard model¹². This is due to the finite extension of the interaction, as well as its dependence on all (three) momenta, and not on the momentum transfer only. By changing to a mixed real-space momentum-space representation, we demonstrate that it can be reduced, for generic momenta, to the inversion of a 52×52 matrix.

Next, in some analogy to the RPA-analysis of the $t - U$ Hubbard model by Schrieffer, Wen, and Zhang¹², we derive the effective two-particle interaction vertex in the static limit, and solve the associated BCS equation. As for the simple Hubbard model studied in Ref. 12, the *d*-wave solution turns out to be the only stable one, in accordance with QMC results. On the other hand, as expected, the *s*-wave solution is unstable, due to the strong on-site Hubbard repulsion U . In the *d*-wave phase, we obtain a decreasing superconducting gap as a function of W , in spite of the fact that the attraction between the quasiparticles should be increased by W . This is due, on the one hand, to the approximation of taking an energy cutoff for the effective interaction, which has been chosen to be of the order of the AF gap, which, in turn, decreases with increasing W . On the other hand, the reduction of the density of states at the Fermi level, which is related to the broadening of the bands produced by W , contributes in reducing the superconducting gap.

Our paper is organized as follows. In Sec. II the $t - U - W$ model with and without phase factors is introduced, and briefly summarized. In Sec. III, we carry out the Hartree-Fock mean-field study of the antiferromagnetic phase. We discuss the HF results and compare them with QMC calculations. In Sec. IV we derive and solve the Bethe-Salpeter equation, i. e. we account for fluctuation effects in the time-dependent HF or generalized RPA scheme. We obtain spin and charge susceptibilities, as well as the effective interaction vertex. In Sec. V, we write down and solve the BCS gap equation, obtained from this effective interaction within a static approximation. Finally, we present our conclusions in Sec. VI, partly based on detailed comparisons with QMC data.

II. MODEL

The Hamiltonian of the $t - U - W$ model is given by⁶

$$\mathcal{H} = -\frac{t}{2} \sum_{\vec{i}} K_{\vec{i}} + U \sum_{\vec{i}} (n_{\vec{i},\uparrow} - \frac{1}{2})(n_{\vec{i},\downarrow} - \frac{1}{2}) - W \sum_{\vec{i}} \tilde{K}_{\vec{i}}^2 \quad (1)$$

with the hopping kinetic energy

$$K_{\vec{i}} = \sum_{\sigma, \vec{\delta}} (c_{\vec{i},\sigma}^\dagger c_{\vec{i}+\vec{\delta},\sigma} + c_{\vec{i}+\vec{\delta},\sigma}^\dagger c_{\vec{i},\sigma}) \quad (2)$$

and

$$\tilde{K}_{\vec{i}} = \sum_{\sigma, \vec{\delta}} f(\vec{\delta}) (c_{\vec{i},\sigma}^\dagger c_{\vec{i}+\vec{\delta},\sigma} + c_{\vec{i}+\vec{\delta},\sigma}^\dagger c_{\vec{i},\sigma}) , \quad (3)$$

where in its original formulation $f(\vec{\delta}) = 1$. As mentioned in the Introduction, this model was introduced by Assaad, Imada, and Scalapino⁶, in order to study the antiferromagnetic-superconducting transition at half filling. As stressed by these authors^{6,7,9,10}, the particular choice of W was mainly motivated formally as a means of introducing the desired quantum transition from the insulating (AF) to the SC state. The choice of the interaction also guaranteed that no fermion-sign problem was encountered in the QMC simulations at half-filling. While there are various approximate ways to physically justify the form of the microscopic Hamiltonian, it runs into problems when directly compared to the high- T_c cuprates. One of the problems of this model is the presence of unphysically broad bands, which also cause problems in the numerical QMC evaluation. For this reason, one of us¹¹ suggested to introduce in the $\tilde{K}_{\vec{i}}$ -term of Eq. (3) a d-wave like phase factor of the form

$$f(\vec{\delta}) = \begin{cases} +1 & \text{for } \vec{\delta} = \pm \vec{a}_x \\ -1 & \text{for } \vec{\delta} = \pm \vec{a}_y \end{cases} . \quad (4)$$

The phase factor restores the correct width of the single-particle bands at $\frac{1}{2}$ -filling. Unfortunately, however no transition to a superconductor in QMC simulations¹¹ has been observed so far.

The W term contains four different processes (see e.g. Ref. 7), among them single-particle terms that renormalize the chemical potential and permit single-particle hopping between second and third nearest-neighbor sites as well as singlet and triplet scattering terms. These terms are not expected to be relevant for the low-energy physics⁷. However, the most interesting term for the quantum phase transition is the fourth term which generates singlet pair-hopping and produces an antiferromagnetic exchange interaction, i. e.

$$\mathcal{H}_W^{(4)} = -2W \sum_{\vec{i}, \vec{\delta}, \vec{\delta}'} f(\vec{\delta}) f(\vec{\delta}') \Delta_{\vec{i}, \vec{\delta}}^\dagger \Delta_{\vec{i}, \vec{\delta}'} , \quad (5)$$

where $\Delta_{\vec{i}, \vec{\delta}}^\dagger = (c_{\vec{i},\uparrow}^\dagger c_{\vec{i}+\vec{\delta},\downarrow}^\dagger - c_{\vec{i},\downarrow}^\dagger c_{\vec{i}+\vec{\delta},\uparrow}^\dagger) / \sqrt{2}$. For $\vec{\delta} = \vec{\delta}'$ the terms in $\mathcal{H}_W^{(4)}$ contribute to the exchange giving:

$$2W \sum_{\vec{i}, \vec{\delta}} (\vec{S}_{\vec{i}} \cdot \vec{S}_{\vec{i}+\vec{\delta}} - \frac{1}{4} n_{\vec{i}} n_{\vec{i}+\vec{\delta}}) . \quad (6)$$

III. HARTREE-FOCK CALCULATIONS

The details of our HF calculation are given in Appendix A. After solving the self-consistent equations for the mean-field parameters in Eqs. (A5) to (A7) and (A20) to (A22) (Appendix A), we arrive at the following results:

Figure 3 displays the free energy of the different phases (antiferromagnetic, superconducting and paramagnetic) for the pure $t - U - W$ model (top) and the $t - U - W$ model with phase factors

(bottom) as a function of W for fixed $U = 4t$ and $T = 0K$. Only the difference to the paramagnetic energy is plotted which is therefore constant.

In the pure $t - U - W$ model (Fig. 3, top) the antiferromagnetic solution (AF) is always the most favorable. However, with increasing W the energy of this solution approaches the paramagnetic solution (PM). The superconducting solution (SC) has a much higher energy than the other solutions. The only possible superconducting solutions have $s_1 = s_3 = 0$ (see Appendix A: no on-site pairing, due to U) and $s_2 \neq 0$ (n. n. singlet pairing), while for $W \lesssim 0.3t$ there exists no superconducting solution. The superconducting order parameter s_2 corresponds to an s-wave like symmetry. The transition from an antiferromagnet to a $d_{x^2-y^2}$ -superconductor observed in QMC simulations are not reproduced at the mean-field level.

In the $t - U - W$ model with phase factors (Fig. 3, bottom) the mean-field ground state is also antiferromagnetic (AF). Here, however, in contrast to the pure $t - U - W$ model, the difference in energy with the paramagnetic (PM) solution is increasing with increasing W . As discussed in Appendix A, there also exist two different superconducting solutions, that lie energetically between the antiferromagnetic and the paramagnetic solution and evolve continuously from the paramagnetic solution at $W = 0t$. In the first solution, s_1 and s_3 are nonvanishing, while $s_2 = 0$ (s-wave). The order parameter has a s-wave symmetry with a superimposed weak modulation of the gap. In the second, energetically more favorable, solution one has $s_1 = s_3 = 0$, and $s_2 \neq 0$, yielding an order parameter with d-wave symmetry. Notice that also in QMC simulations at half-filling, no transition to a superconductor was found in the $t - U - W$ model with phase factors, in agreement with our results. However, the mean-field result in Fig. 3 is promising in direction of doping away from half-filling, where the AF phase is suppressed.

The band structure of the antiferromagnetic solutions is evaluated along the usual paths through the Brillouin zone, as shown in Fig. 4.

Fig. 5 (top) gives the bands of the pure $t - U - W$ model for $W = 0.15t$. One can recognize easily that the bands are much wider than in the Hubbard model but their shape is nearly unaltered. This means that if one would scale the bands by a factor $\frac{1}{3}$, they would be almost identical. The effect of W seems thus to be a mere “dilatation” of the bands.

In the $t - U - W$ model with phase factors, things look quite different. The bands are plotted in Fig. 5 (middle) along the path shown in Fig. 4(a) and in Fig. 5 (bottom) along the path shown in Fig. 4(b) with $W = 0.05t$. The width of the bands is nearly the same as in the Hubbard model, except for the lifting of the degeneracy along the boundaries of the magnetic Brillouin zone (MBZ). At $\vec{k} = (\pi, 0)$ a kind of double-hump structure can be seen like it appears in t - t' - t'' models to describe high- T_c superconductors¹⁴. This can be explained as follows: The W term contains also hopping processes to second and third nearest neighbor sites^{7,11} which, due to the phase factors, have the same sign as in the standard fit parameters t, t', t'' which are often used to adjust the bands to the experimental data of $\text{Bi}_2\text{Sr}_2\text{CaCu}_2\text{O}_{8+\delta}$ and $\text{YBa}_2\text{Cu}_3\text{O}_{7-\delta}$.

If one compares the antiferromagnetic bands to the QMC data^{10,11,15} of the $t - U - W$ model as in Figs. 6 and 7, one gets a very good agreement. The width of the bands as well as the antiferromagnetic gap were reproduced excellently. In addition, the energy bands of the $t - U - W$ model with phase factors (Fig. 5) show the same double-hump structure at $\vec{k} = (\pi, 0)$ like it is seen in the QMC spectral weight $A(\vec{k}, \omega)$ (Fig. 7). They also reproduce well the lift of the degeneracy along the boundaries of the MBZ.

Finally, we want to look at two characteristic features of the antiferromagnetic solution: the sublattice magnetization m and the Mott-Hubbard gap. The sublattice magnetization defined as

$$m = |\langle c_{\vec{i},\uparrow}^\dagger c_{\vec{i},\uparrow} \rangle - \langle c_{\vec{i},\downarrow}^\dagger c_{\vec{i},\downarrow} \rangle|, \quad (7)$$

is plotted in Fig. 8 (top) as a function of W . As expected from the behavior of the free energy (Fig. 3), the sublattice magnetization decreases with increasing W in the pure $t - U - W$ model. On the other hand, the sublattice magnetization of the $t - U - W$ model with phase factors is getting stronger with increasing W . This is also confirmed by QMC data¹¹, which show an amplification of the antiferromagnetic correlations with increasing W .

A similar picture occurs for the antiferromagnetic gap (Fig. 8, bottom). Like the sublattice magnetization, the Mott-Hubbard gap is decreasing with increasing W in the pure $t - U - W$ model, while it increases (nearly linear) with W in the model with phase factors.

In summary, the Hartree-Fock calculations give the antiferromagnetic solution as ground state for any values of W in both models. However, qualitatively there are remarkable differences between

the two models with and without phase factors. A comparison of these results with the QMC data shows that the antiferromagnetic phase is described quite well by the mean-field approximation.

On the other hand, the mean-field level is not able to reproduce the transition to a $d_{x^2-y^2}$ -superconductor at $W_c \approx 0.3t$ observed in QMC simulations in the pure $t - U - W$ model. Nevertheless, for large W , for which the AF gap becomes small, one would expect the antiferromagnetic solution to become unstable with respect to fluctuations beyond the mean-field level. This is what we analyze in the next section.

IV. TIME-DEPENDENT HARTREE-FOCK (GENERALIZED RPA)

As demonstrated in the previous section, the HF mean-field approximation is not sufficient to describe the transition to a $d_{x^2-y^2}$ -superconductor occurring in the pure $t - U - W$ model according to QMC simulations. For that reason, we carried out an improved calculation, including charge- and spin-density fluctuations. This has been done by means of a time-dependent HF or generalized random phase approximation (RPA), in which we summed both "bubble" and "ladder" particle-hole diagrams. In contrast to the fluctuation exchange approximation (FLEX), the Green's function are not calculated selfconsistently, but taken over from the Hartree-Fock results, as it has been done in Ref. 12.

A. Hartree-Fock Correlation Function L^0 and Interaction Vertex Γ^0

The 2×2 antiferromagnetic Hartree-Fock Green's function can be written as (see Appendix A, Eqs. (A4) to (A12)):

$$\mathcal{G}^{HF}(\vec{k}, \omega, \sigma) = \begin{pmatrix} i\omega + \varepsilon(\vec{k}) & \sigma\Delta(\vec{k}) \\ \sigma\Delta(\vec{k}) & i\omega - \varepsilon(\vec{k}) \end{pmatrix} \frac{1}{-\omega^2 - E^2(\vec{k})}. \quad (8)$$

With this Green's function we can construct the Hartree-Fock two-particle propagator L^0 :

$$L_{\sigma_1 \sigma_2}^{0 \frac{m_1 m_2}{m'_1 m'_2}}(\vec{k}_1, \vec{k}_2, \vec{q}, \omega_1, \omega_2, \nu) = \delta_{\sigma_1 \sigma_2} \delta_{\sigma'_1 \sigma'_2} \delta_{\vec{k}_1 \vec{k}_2} \delta_{\omega_1 \omega_2} \mathcal{G}^{HF}{}_{m_2 m_1}(\vec{k}_1, \omega_1, \sigma_1) \mathcal{G}^{HF}{}_{m'_1 m'_2}(\vec{k}_1 - \vec{q}, \omega_1 - \nu, \sigma'_1), \quad (9)$$

where the set of m_i stand for the indices of the 2×2 matrix in Eq. (8). After a unitary transformation with help of the Pauli matrices, i. e.

$$\tilde{L}^0 = U^\dagger L^0 U, \quad (10)$$

where

$$U_{\sigma_2 \alpha} = \frac{1}{\sqrt{2}} \sigma_{\sigma_1 \sigma_2}^\alpha, \quad \alpha = 0, x, y, z, \quad (11)$$

we can write the correlation function in the charge-/ spin-channel representation as:

$$\tilde{L}_{a b}^{0 \frac{m_1 m_2}{m'_1 m'_2}}(k_1, k_2, q) = \begin{pmatrix} \tilde{L}_{00}^{0 \frac{m_1 m_2}{m'_1 m'_2}}(k_1, k_2, q) & 0 & 0 & \tilde{L}_{0z}^{0 \frac{m_1 m_2}{m'_1 m'_2}}(k_1, k_2, q) \\ 0 & \tilde{L}_{+-}^{0 \frac{m_1 m_2}{m'_1 m'_2}}(k_1, k_2, q) & 0 & 0 \\ 0 & 0 & \tilde{L}_{-+}^{0 \frac{m_1 m_2}{m'_1 m'_2}}(k_1, k_2, q) & 0 \\ \tilde{L}_{z0}^{0 \frac{m_1 m_2}{m'_1 m'_2}}(k_1, k_2, q) & 0 & 0 & \tilde{L}_{zz}^{0 \frac{m_1 m_2}{m'_1 m'_2}}(k_1, k_2, q) \end{pmatrix}. \quad (12)$$

Here and in the following: $k = (\vec{k}, \omega)$, $q = (\vec{q}, \nu)$ and so on.

In contrast to the Hubbard model, also the non-diagonal elements which couple the charge channel to the longitudinal spin channel have to be taken into account. For the following calculations it is also advantageous to transform from the representation

$$\tilde{L}_{ab}^0 \stackrel{m_1 m_2}{m'_1 m'_2}(\vec{k}_1, \vec{k}_2, \vec{q}, \omega_1, \omega_2, \nu) \quad \text{with} \quad \vec{k}_1, \vec{k}_2, \vec{q} \in MBZ \quad (13)$$

to the representation

$$\overline{L}_{ab}^0(\vec{k}_1, \vec{k}_2, \omega_1, \omega_2; \vec{q} + n\vec{Q}, \vec{q} + n'\vec{Q}, \nu) \quad \text{with} \quad \vec{k}_1, \vec{k}_2 \in BZ, \quad \vec{q} \in MBZ, \quad (14)$$

where n, n' take the values $\{0, 1\}$ and $\vec{Q} = (\pi, \pi)$.

In this representation, e. g., the longitudinal spin correlation function can be written as a matrix in the indices n, n' :

$$\overline{L}_{zz}^0(k_1, k_2; \vec{q} + n\vec{Q}, \vec{q} + n'\vec{Q}, \nu) = \delta_{\omega_1 \omega_2} \begin{pmatrix} \tilde{\mathcal{G}}_{11}^{HF}(k_1) \tilde{\mathcal{G}}_{11}^{HF}(k_1 - q) + \delta_{\vec{k}_1 \vec{k}_2 + \vec{Q}} \tilde{\mathcal{G}}_{21}^{HF}(k_1) \tilde{\mathcal{G}}_{12}^{HF}(k_1 - q) & 0 \\ 0 & \delta_{\vec{k}_1 \vec{k}_2} \tilde{\mathcal{G}}_{11}^{HF}(k_1) \tilde{\mathcal{G}}_{22}^{HF}(k_1 - q) + \delta_{\vec{k}_1 \vec{k}_2 + \vec{Q}} \tilde{\mathcal{G}}_{21}^{HF}(k_1) \tilde{\mathcal{G}}_{21}^{HF}(k_1 - q) \end{pmatrix}. \quad (15)$$

Here the $\tilde{\mathcal{G}}^{HF}$ are spin independent Green's functions (i. e. \mathcal{G}^{HF} (Eq. (8)) with spin index σ set equal to $+1$). The interaction vertex in this representation is given by

$$\begin{aligned} \overline{\Gamma}_{ab}^0(\vec{k}_1, \vec{k}_2; \vec{q} + n\vec{Q}, \vec{q} + n'\vec{Q}) = & \frac{1}{\beta N} \{ \begin{pmatrix} 1 & 0 & 0 & 0 \\ 0 & -1 & 0 & 0 \\ 0 & 0 & -1 & 0 \\ 0 & 0 & 0 & -1 \end{pmatrix} \otimes \begin{pmatrix} 1 & 0 \\ 0 & 1 \end{pmatrix} U \\ & + \begin{pmatrix} 2 & 0 & 0 & 0 \\ 0 & 0 & 0 & 0 \\ 0 & 0 & 0 & 0 \\ 0 & 0 & 0 & 0 \end{pmatrix} \otimes [\begin{pmatrix} 1 & 0 \\ 0 & 0 \end{pmatrix} V^W(\vec{k}_2 - \vec{q}, \vec{k}_1, \vec{q}) \\ & \quad + \begin{pmatrix} 0 & 0 \\ 0 & -1 \end{pmatrix} V^W(\vec{k}_2 - \vec{q}, \vec{k}_1, \vec{q} + \vec{Q})] \\ & - \begin{pmatrix} 1 & 0 & 0 & 0 \\ 0 & 1 & 0 & 0 \\ 0 & 0 & 1 & 0 \\ 0 & 0 & 0 & 1 \end{pmatrix} \otimes \begin{pmatrix} 1 & 0 \\ 0 & -1 \end{pmatrix} V^W(\vec{k}_2 - \vec{q}, \vec{k}_1, \vec{k}_1 - \vec{k}_2) \}. \end{aligned} \quad (16)$$

It is written as a direct product of spin- and (n, n') -matrices with the W -dependent interaction V^W given in Appendix B, Eq. (B1).

B. Bethe-Salpeter Equation

With help of the HF two-particle propagator \overline{L} and the interaction vertex $\overline{\Gamma}$, we can now write down the Bethe-Salpeter equation in the form:

$$\begin{aligned} \overline{L}_{ab}(k_1, k_2; \vec{q}, \vec{q}', \nu) = & \overline{L}_{ab}^0(k_1, k_2; \vec{q}, \vec{q}', \nu) \\ & + \sum_{\substack{k_3, k_4 \\ \vec{q}'', \vec{q}'' \\ c, d}} \overline{L}_{ac}^0(k_1, k_3; \vec{q}, \vec{q}'', \nu) \overline{\Gamma}_{cd}^0(\vec{k}_3, \vec{k}_4; \vec{q}'', \vec{q}''') \overline{L}_{db}(k_4, k_2; \vec{q}''', \vec{q}', \nu). \end{aligned} \quad (17)$$

Unlike for the standard ($W = 0$) Hubbard model, this equation cannot be easily inverted due to the complicated space and spin structure of the W term. For this reason, we apply a method due to Hanke and Sham¹⁷, which is based on the partial transformation of the interaction vertex back

into real space. For short-range interactions, this yields finite (small-sized) matrices in real space. With the Fourier-transformed correlation function and interaction vertex

$$\widehat{L}_{ab}(\vec{R}_1, \vec{R}_2; \vec{q}, \vec{q}', \nu) = -\frac{1}{\beta N} \sum_{\substack{\vec{k}_1, \vec{k}_2 \\ \omega_1, \omega_2}} e^{i\vec{k}_1 \vec{R}_1} e^{-i\vec{k}_2 \vec{R}_2} \overline{L}_{ab}(k_1, k_2; \vec{q}, \vec{q}', \nu), \quad (18)$$

$$\widehat{\Gamma}_{ab}^0(\vec{R}_1, \vec{R}_2; \vec{q}, \vec{q}') = -\frac{\beta}{N} \sum_{\vec{k}_1, \vec{k}_2} e^{i\vec{k}_1 \vec{R}_1} e^{-i\vec{k}_2 \vec{R}_2} \overline{\Gamma}_{ab}^0(\vec{k}_1, \vec{k}_2; \vec{q}, \vec{q}'), \quad (19)$$

we obtain the Bethe-Salpeter equation in matrix form:

$$\begin{aligned} \widehat{L}_{ab}(\vec{R}_1, \vec{R}_2; \vec{q}, \vec{q}', \nu) = & \widehat{L}_{ab}^0(\vec{R}_1, \vec{R}_2; \vec{q}, \vec{q}', \nu) \\ & + \widehat{L}_{ac}^0(\vec{R}_1, \vec{R}_3; \vec{q}, \vec{q}'', \nu) \widehat{\Gamma}_{cd}^0(\vec{R}_3, \vec{R}_4; \vec{q}'', \vec{q}''') \widehat{L}_{db}(\vec{R}_4, \vec{R}_2; \vec{q}''', \vec{q}', \nu). \end{aligned} \quad (20)$$

This is now a simple matrix equation which can easily be inverted for the interacting two-particle propagator \widehat{L} :

$$\widehat{L} = \left(1 - \widehat{L}^0 \widehat{\Gamma}^0 \right)^{-1} \widehat{L}^0. \quad (21)$$

In contrast to the Hubbard model we have to deal with complex 26×26 matrices for the transverse spin-channel and with complex 52×52 matrices for the coupled charge-/ longitudinal spin-channel. The RPA susceptibilities can be constructed by taking the $(\vec{0}, \vec{0})$ -matrix element in real space, i. e.:

$$\chi_{ab}(\vec{q}, \vec{q}'; \nu) = \widehat{L}_{ab}(\vec{0}, \vec{0}; \vec{q}, \vec{q}', \nu). \quad (22)$$

From this one obtains the retarded susceptibilities by the analytic continuation $i\nu \rightarrow \omega + i\eta$.

Starting from the idea that spin fluctuations are responsible for the pairing of the quasi-particles, it is reasonable to first concentrate on the dynamic spin susceptibilities for the antiferromagnetic nesting vector $\vec{Q} = (\pi, \pi)$ as a function of ω , as we expect the strongest response there. In Fig. 9 (top), χ_{zz} is plotted for the pure $t - U - W$ model with $W = 0.1t$, while in Fig. 9 (middle) χ_{zz} is displayed for the model with phase factors and $W = 0.05t$. Both calculations can be compared with the result for the Hubbard model, reported in Fig. 9 (bottom).

One can clearly see that the spectral weight is mainly concentrated at low frequencies and that it is abruptly decreasing at a frequency $\omega \approx 2\Delta_{AF}$, which corresponds to the antiferromagnetic gap. This behavior is most evident in the pure $t - U - W$ model. Moreover, one can recognize that the overall magnitude of the longitudinal spin susceptibility is biggest in the pure $t - U - W$ model and smallest in the $t - U - W$ model with phase factors.

C. Effective Interaction

In this section, we calculate the effective 2-particle interaction mediated by the collective charge and spin fluctuations evaluated in the preceding section. Here, we restrict to the model without phase factor, since this is the only one which, according to QMC calculations, displays d -wave superconductivity. As a first step, we evaluate the fluctuation vertex, from which we can determine the modifications of the bare 2-particle interaction given by the $t - U - W$ Hamiltonian. The calculation of the fluctuation vertex is performed with the same techniques that were used to calculate the Bethe-Salpeter equation. This gives the expression:

$$\begin{aligned} \overline{\Gamma}_{ab}(\vec{k}_1, \vec{k}_2; \vec{q}, \vec{q}', \nu) = & \sum_{\substack{k_3, k_4 \\ \vec{q}'', \vec{q}''' \\ c, d}} \overline{\Gamma}_{ac}^0(\vec{k}_1, \vec{k}_3; \vec{q}, \vec{q}'') \overline{L}_{cd}(k_3, k_4; \vec{q}'', \vec{q}''', \nu) \overline{\Gamma}_{db}^0(\vec{k}_4, \vec{k}_2; \vec{q}''', \vec{q}') \\ = & \sum_{\substack{\vec{R}_1, \vec{R}_2 \\ \vec{R}_3, \vec{R}_4}} \sum_{\substack{\vec{q}'', \vec{q}''' \\ c, d}} \left(\frac{-1}{\beta N} \right) e^{-i\vec{k}_1 \vec{R}_1} \widehat{\Gamma}_{ac}^0(\vec{R}_1, \vec{R}_3; \vec{q}, \vec{q}'') \\ & \cdot \widehat{L}_{cd}(\vec{R}_3, \vec{R}_4; \vec{q}'', \vec{q}''', \nu) \widehat{\Gamma}_{db}^0(\vec{R}_4, \vec{R}_2; \vec{q}''', \vec{q}') e^{i\vec{k}_2 \vec{R}_2}, \end{aligned} \quad (23)$$

which is diagrammatically represented in Fig. 1.

Next, we have to change from the charge/spin channel representation back to the pure spin representation by inverting the transformation given by Eq. (10):

$$\begin{aligned}
\Gamma^{\sigma_1 \sigma_2}_{\sigma'_1 \sigma'_2}(\vec{k}_1, \vec{k}_2; \vec{q}, \vec{q}', \nu) &= U^{\sigma_1}_{\sigma'_1 a} \bar{\Gamma}_{a b}(\vec{k}_1, \vec{k}_2; \vec{q}, \vec{q}', \nu) (U^{\sigma_2}_{\sigma'_2 b})^\dagger \\
&= \frac{1}{2} (\bar{\Gamma}_{00}(\vec{k}_1, \vec{k}_2; \vec{q}, \vec{q}', \nu) \sigma^0_{\sigma_1 \sigma'_1} \sigma^0_{\sigma'_2 \sigma_2} + \bar{\Gamma}_{0z}(\vec{k}_1, \vec{k}_2; \vec{q}, \vec{q}', \nu) \sigma^0_{\sigma_1 \sigma'_1} \sigma^z_{\sigma'_2 \sigma_2} \\
&\quad + \bar{\Gamma}_{z0}(\vec{k}_1, \vec{k}_2; \vec{q}, \vec{q}', \nu) \sigma^z_{\sigma_1 \sigma'_1} \sigma^0_{\sigma'_2 \sigma_2} + \bar{\Gamma}_{zz}(\vec{k}_1, \vec{k}_2; \vec{q}, \vec{q}', \nu) \sigma^z_{\sigma_1 \sigma'_1} \sigma^z_{\sigma'_2 \sigma_2} \\
&\quad + \bar{\Gamma}_{+-}(\vec{k}_1, \vec{k}_2; \vec{q}, \vec{q}', \nu) \tilde{\sigma}^-_{\sigma_1 \sigma'_1} \tilde{\sigma}^+_{\sigma'_2 \sigma_2} + \bar{\Gamma}_{-+}(\vec{k}_1, \vec{k}_2; \vec{q}, \vec{q}', \nu) \tilde{\sigma}^+_{\sigma_1 \sigma'_1} \tilde{\sigma}^-_{\sigma'_2 \sigma_2}).
\end{aligned} \tag{24}$$

Since we want to use the effective interaction in order to write an effective Hamiltonian, only the static limit of the fluctuation vertex has to be considered. Thus, simple diagrammatic rules¹⁶ yield for the correction to the bare interaction:

$$\tilde{V}^{\sigma_1 \sigma_2}_{\sigma'_1 \sigma'_2}(\vec{k}_1, \vec{k}_2; \vec{q}, \vec{q}') = \Gamma^{\sigma_1 \sigma_2}_{\sigma'_1 \sigma'_2}(\vec{k}_1, \vec{k}_2; \vec{q}, \vec{q}', 0) \cdot (-\beta N) \cdot (-1). \tag{25}$$

The effective interaction can then be written as (see Fig. 2 for diagrammatic representation)

$$V_{eff}^{\sigma_1 \sigma_2}_{\sigma'_1 \sigma'_2}(\vec{k}_1, \vec{k}_2; \vec{q}, \vec{q}') = V^{\sigma_1 \sigma_2}_{\sigma'_1 \sigma'_2}(\vec{k}_1, \vec{k}_2; \vec{q}) + \tilde{V}^{\sigma_1 \sigma_2}_{\sigma'_1 \sigma'_2}(\vec{k}_1, \vec{k}_2; \vec{q}, \vec{q}') \tag{26}$$

with the bare 2-particle interaction

$$V^{\sigma_1 \sigma_2}_{\sigma'_1 \sigma'_2}(\vec{k}_1, \vec{k}_2; \vec{q}) = U \delta_{\sigma_1 \sigma'_1} \delta_{\sigma_2 \sigma'_2} \delta_{\sigma_1 \sigma_2} + V^W(\vec{k}_2 - \vec{q}, \vec{k}_1; \vec{q}) \delta_{\sigma_1 \sigma'_1} \delta_{\sigma_2 \sigma'_2} \tag{27}$$

and V^W given by Eq. (B1) (Appendix B). Since one has to consider the pairing of the Hartree-Fock quasiparticles, the effective interaction has to be transformed into the γ -base, which produces additional coherence factors¹².

For physical reasons, only the pairing of particles with opposite spin (singlet-pairing) was considered. In order to take into account the effect of the dynamics on top of our static approximation, we follow Ref. 12, and introduce a cutoff frequency ω_c , analogous to the Debye frequency ω_D in the standard BCS theory. This ensures that only particles within an interval of width $\hbar \omega_c$ above and below the Fermi energy E_F are paired.

The motivation for this cutoff frequency ω_c becomes clear if one looks at the spin susceptibilities of the pure $t - U - W$ model in Fig. 9. We have already shown in the preceding section that the spectral weight is concentrated at low frequencies. Under the condition that the spin fluctuations are responsible for the pairing of the quasi-particles, the longitudinal spin susceptibility gives quite naturally a cutoff frequency of the size of the antiferromagnetic gap ($\omega_c \approx 2\Delta_{AF}$).

This implies that for hole dopings away from half-filling, only the intra-valence band matrix elements have to be considered. The pairing part of the effective Hamiltonian can thus formally be written as

$$\mathcal{H}^{pair} = \frac{1}{2N} \sum'_{\vec{k}, \vec{k}'} V_{\sigma \sigma'}^{pair}(\vec{k}, \vec{k}') \Theta(\omega_c - |E^v(\vec{k}) - E_F|) \Theta(\omega_c - |E^v(\vec{k}') - E_F|) \gamma_{\vec{k}', \sigma'}^{v\dagger} \gamma_{-\vec{k}', -\sigma'}^{v\dagger} \gamma_{-\vec{k}, -\sigma}^v \gamma_{\vec{k}, \sigma}^v, \tag{28}$$

where $E^v(\vec{k}) = -E(\vec{k})$ is the valance band energy.

The direct interaction $V_{\sigma \sigma'}^{pair}(\vec{k}, \vec{k}')$, which is given by $\sigma = \sigma'$ spin indices contains, besides the longitudinal spin fluctuations, also the bare interactions and the charge fluctuations. The exchange interaction with $\sigma = -\sigma'$ consists of the transverse spin fluctuations only. In Figs. 10 to 12, the direct interaction and the exchange interaction were plotted for different paths of \vec{k} and \vec{k}' through the magnetic Brillouin zone (MBZ) for the pure $t - U - W$ model and the Hubbard model, respectively. The exchange interaction was plotted there as $-V_{\sigma - \sigma'}^{pair}(\vec{k}, -\vec{k}')$, since it has exactly this form, with negative sign, in the BCS gap equation (see Eq. (30)).

Comparing the graphs for the pure $t - U - W$ model ($W = 0.1t$) with the pure Hubbard model, one can easily see that the W term amplifies the attractive parts of the direct interaction, whereas the attractive parts of the exchange interaction remain constant (see e. g. Fig. 11). However, the repulsive parts of the direct interaction and the exchange interaction were both attenuated considerably by increasing W (see e. g. Fig. 12). Therefore, the pairing of the quasi-particles is favored in the pure $t - U - W$ model altogether.

V. BCS GAP EQUATION

Finally, we want to solve the BCS gap equation for the effective pairing interaction. Starting point is the effective Hamiltonian, as obtained in the previous Section

$$\begin{aligned} \mathcal{H}_{eff} = & \sum'_{\vec{k}, \sigma} (E^v(\vec{k}) - \mu) \gamma_{\vec{k}, \sigma}^{v\dagger} \gamma_{\vec{k}, \sigma}^v \\ & + \frac{1}{2N} \sum'_{\substack{\vec{k}, \vec{k}' \\ \sigma, \sigma'}} V_{\sigma \sigma'}^{pair}(\vec{k}, \vec{k}') \Theta(\omega_c - |E^v(\vec{k}) - E_F|) \Theta(\omega_c - |E^v(\vec{k}') - E_F|) \gamma_{\vec{k}', \sigma'}^{v\dagger} \gamma_{-\vec{k}', -\sigma'}^{v\dagger} \gamma_{-\vec{k}, -\sigma}^v \gamma_{\vec{k}, \sigma}^v. \end{aligned} \quad (29)$$

With this Hamiltonian we want to study the superconducting properties of the pure $t - U - W$ model for different hole doping and different values of the model parameter W . The BCS gap equation becomes

$$\Delta(\vec{k}) = -\frac{1}{N} \sum'_{\vec{k}'} (V_{\uparrow\uparrow}(\vec{k}, \vec{k}') - V_{\uparrow\downarrow}(\vec{k}, -\vec{k}')) \frac{\Delta(\vec{k}')}{2E(\vec{k}')}. \quad (30)$$

Here we used the abbreviations

$$E(\vec{k}) = \sqrt{\xi^2(\vec{k}) + \Delta^2(\vec{k})}, \quad (31)$$

$$\xi(\vec{k}) = E^v(\vec{k}) - \mu, \quad (32)$$

$$V_{\sigma \sigma'}(\vec{k}, \vec{k}') = V_{\sigma \sigma'}^{pair}(\vec{k}, \vec{k}') \Theta(\omega_A - |E^v(\vec{k}) - E_F|) \Theta(\omega_A - |E^v(\vec{k}') - E_F|). \quad (33)$$

The gap equation (30) was iterated by assuming different symmetries of the superconducting order parameter, however, only d -wave solutions turn out to converge.

The results are shown in Fig. 13. There are two striking observations: first, there are oscillations in the superconducting gap function that increase with W , and second, the superconducting gap decreases with W . The oscillations are an effect of the small lattice size, which has an increasing finite-size effect at small cutoff frequencies and thus bigger W -values (see Fig. 8). However, these oscillations change none of the qualitative remarks made below.

It remains the question why the superconducting gap is getting smaller with increasing W , in spite of the fact that the bare attraction between the quasi-particles is enhanced by the W term. To understand this, one has to keep in mind that there are other important quantities, like the cutoff frequency or the density of states at the Fermi level, which have an important effect on the magnitude of the superconducting gap. How the superconducting gap depends on these quantities is qualitatively seen already in the weak-coupling solution of the original BCS equation for an attractive δ -potential¹⁶:

$$\Delta = 2\hbar\omega_D \exp\left(-\frac{1}{N(0)g}\right). \quad (34)$$

A stronger coupling g is increasing the superconducting gap, while a smaller cutoff frequency ω_D is decreasing it. Moreover, if the density of states at the Fermi level $N(0)$ is reduced, the superconducting gap is getting smaller, as well. This final point is decisive, since the W term is broadening the energy bands considerably, thus reducing the density of states dramatically. Therefore, the fact that the superconducting gap is getting smaller with increasing W can be understood within our approximation.

VI. COMPARISON WITH QMC RESULTS AND CONCLUSIONS

In this paper, we have first shown that the standard Hartree-Fock approximation can describe the antiferromagnetic properties of the $t - U - W$ model, especially the single-particle energy bands, in surprisingly good agreement with the QMC simulations. On the other hand, it is unable to reproduce the transition to a d -wave superconductor observed in the pure $t - U - W$ model in numerical simulations (QMC). This short-coming is overcome in the time-dependent HF or generalized RPA calculations, presented in the second part of our paper.

The standard Hartree-Fock approximation captures only the “high-energy” physics, and is thus capable of reproducing band-widths and the overall features of the single-particle spectral-function. Equivalently, short-range pairing-correlation functions should be well reproduced within this approximation. This is indeed the case. At short length scales (as shown in table 1) the extended s-wave vertex contribution to the pairing correlation functions is dominant in QMC simulations of the pure t - U - W model. It is only at *larger* distances that the d -wave pairing correlations become dominant. This crossover from *short range* to *long range* properties is not reproduced within the standard mean-field approximation. Alternatively, for the t - U - W model with phase factors d -wave pairing dominates in QMC simulations at small length scales (see table 2).

On the other hand, by including charge and spin fluctuations within a time-dependent HF, or generalized RPA summation of ladder and bubble diagrams, we were able to demonstrate that the attraction between the quasi-particles is enhanced by W and that the corresponding superconducting order parameter displays the correct d -wave symmetry.

The QMC results indeed show that as W increases at fixed U or U decreases at fixed W , an instability towards d -wave superconductivity occurs. To illustrate this, Fig. 14 plots the vertex contribution to the d -wave pairing correlations as well as the staggered spin susceptibility. As apparent at low U for fixed W , the superconducting d -wave becomes the leading instability.

ACKNOWLEDGMENTS

The authors express their deep gratitude to Prof. M. Imada for many insightful discussions and clarifications of physical points. In this connection one of us (W. H.) is grateful to Prof. Imada for the warm hospitality experienced during visits at the ISSP in Tokyo. He acknowledges the support granted by the joint German - Japanese cooperation project (DFG - JSPS: 446 JAP - 113/114/0), which was central for the success of this work.

APPENDIX A: DETAILS OF THE HF CALCULATIONS

1. Antiferromagnetic Mean Field

We start with the following Ansatz for the mean field parameters:

$$\langle c_{\vec{i},\sigma}^\dagger c_{\vec{i},\sigma} \rangle = n_1 + \sigma e^{i\vec{Q} \cdot \vec{i}} n_2, \quad (\text{A1})$$

$$\langle c_{\vec{i},\sigma}^\dagger f(\vec{\delta}) c_{\vec{i}+\vec{\delta},\sigma} \rangle = n_3, \quad (\text{A2})$$

$$\langle c_{\vec{i}+\vec{\delta},\sigma}^\dagger f(\vec{\delta}) f(\vec{\delta}') c_{\vec{i}+\vec{\delta}',\sigma} \rangle = n_4 + \sigma e^{i\vec{Q} \cdot \vec{i}} n_5, \quad (\text{A3})$$

where \vec{Q} denotes the antiferromagnetic nesting-vector $\vec{Q} = (\pi, \pi)$. Here the expectation values $\langle \dots \rangle$ contain also an average over all $\vec{\delta}$ and $\vec{\delta}'$, whenever explicitly present. At half filling, it is easy to show that $n_1 = \frac{1}{2}$, and $n_4 = \frac{1}{8}$. The mean-field Hamiltonian can then be written as

$$\mathcal{H}_{tUW}^{MF} = \sum'_{\vec{k},\sigma} (\tilde{c}_{\vec{k},\sigma}^\dagger, \tilde{c}_{\vec{k}+\vec{Q},\sigma}^\dagger) \begin{pmatrix} \varepsilon(\vec{k}) & \sigma\Delta(\vec{k}) \\ \sigma\Delta(\vec{k}) & -\varepsilon(\vec{k}) \end{pmatrix} \begin{pmatrix} \tilde{c}_{\vec{k},\sigma} \\ \tilde{c}_{\vec{k}+\vec{Q},\sigma} \end{pmatrix} + \tilde{E}_{tUW}^{MF} \quad (\text{A4})$$

with

$$\varepsilon(\vec{k}) = -2t(\cos k_x + \cos k_y) - 96Wn_3(\cos k_x \pm \cos k_y), \quad (\text{A5})$$

$$\Delta(\vec{k}) = -Un_2 + 32Wn_5 - 8Wn_2(\cos k_x \pm \cos k_y)^2 \quad (\text{A6})$$

and

$$\tilde{E}_{tUW}^{MF} = +UNn_2^2 + 192WNn_3^2 - 64WN(\frac{1}{16} + n_2n_5). \quad (\text{A7})$$

Here, and in the following equations, the upper sign stands for the pure $t - U - W$ model, while the lower sign is used for the $t - U - W$ model with phase factors. The Hamiltonian can be diagonalized by the usual transformation

$$\begin{pmatrix} \gamma_{\vec{k},\sigma}^c \\ \gamma_{\vec{k},\sigma}^v \end{pmatrix} = \begin{pmatrix} u(\vec{k}) & \sigma v(\vec{k}) \\ v(\vec{k}) & -\sigma u(\vec{k}) \end{pmatrix} \begin{pmatrix} \tilde{c}_{\vec{k},\sigma} \\ \tilde{c}_{\vec{k}+\vec{Q},\sigma} \end{pmatrix} \quad (\text{A8})$$

with

$$u(\vec{k}) = \left[\frac{1}{2} \left(1 + \frac{\varepsilon(\vec{k})}{E(\vec{k})} \right) \right]^{\frac{1}{2}}, \quad (\text{A9})$$

$$v(\vec{k}) = \left[\frac{1}{2} \left(1 - \frac{\varepsilon(\vec{k})}{E(\vec{k})} \right) \right]^{\frac{1}{2}} \quad (\text{A10})$$

and

$$E(\vec{k}) = \sqrt{\varepsilon^2(\vec{k}) + \Delta^2(\vec{k})}. \quad (\text{A11})$$

The resulting Hamiltonian is given by

$$\mathcal{H}_{tUW}^{MF} = \sum_{\vec{k},\sigma}' E(\vec{k}) (\gamma_{\vec{k},\sigma}^{c\dagger} \gamma_{\vec{k},\sigma}^c - \gamma_{\vec{k},\sigma}^{v\dagger} \gamma_{\vec{k},\sigma}^v) + \tilde{E}_{tUW}^{MF}. \quad (\text{A12})$$

Already at this point, one can see from equations (A5) and (A11) that the parameter n_3 produces extremely wide bands in the pure $t - U - W$ model. On the other hand, it is straightforward to see that for the alternative $t - U - W$ model with phase factors one must have $n_3 \equiv 0$, in order to preserve the symmetry of the energy bands under interchange of x- and y-directions. This explains why the bandwidth of the $t - U - W$ model with phase factors is drastically smaller, and essentially the same as the one of the pure Hubbard model.

2. Superconducting Mean Field

Here, the mean field parameters are chosen as:

$$\langle c_{\vec{i},\sigma}^\dagger c_{\vec{i},\sigma} \rangle = n_1, \quad (\text{A13})$$

$$\langle c_{\vec{i},\sigma}^\dagger f(\vec{\delta}) c_{\vec{i}+\vec{\delta},\sigma} \rangle = n_3, \quad (\text{A14})$$

$$\langle c_{\vec{i}+\vec{\delta},\sigma}^\dagger f(\vec{\delta}) f(\vec{\delta}') c_{\vec{i}+\vec{\delta}',\sigma} \rangle = n_4, \quad (\text{A15})$$

$$\langle c_{\vec{i},\sigma}^\dagger c_{\vec{i},-\sigma}^\dagger \rangle = \sigma s_1, \quad (\text{A16})$$

$$\langle c_{\vec{i},\sigma}^\dagger f(\vec{\delta}) c_{\vec{i}+\vec{\delta},-\sigma}^\dagger \rangle = \sigma s_2, \quad (\text{A17})$$

$$\langle c_{\vec{i}+\vec{\delta},\sigma}^\dagger f(\vec{\delta}) f(\vec{\delta}') c_{\vec{i}+\vec{\delta}',-\sigma}^\dagger \rangle = \sigma s_3. \quad (\text{A18})$$

The superconducting parameters can be divided into two groups: s_2 stands for the nearest-neighbor singlet pairing, which is favored by the W term (Eq. (5)). On the other hand, s_1 and s_3 for $\delta = \delta'$

represent the on-site singlet pairing which is suppressed by the Hubbard U . The mean-field Hamiltonian thus is

$$\mathcal{H}_{tUW}^{MF} = \sum_{\vec{k}} (\tilde{c}_{\vec{k},\uparrow}^\dagger, \tilde{c}_{-\vec{k},\downarrow}) \begin{pmatrix} \varepsilon(\vec{k}) & \Delta(\vec{k}) \\ \Delta(\vec{k}) & -\varepsilon(\vec{k}) \end{pmatrix} \begin{pmatrix} \tilde{c}_{\vec{k},\uparrow} \\ \tilde{c}_{-\vec{k},\downarrow}^\dagger \end{pmatrix} + \tilde{E}_{tUW}^{MF} \quad (\text{A19})$$

with the single-particle energy $\varepsilon(\vec{k})$ and the gap parameter $\Delta(\vec{k})$ given by:

$$\begin{aligned} \varepsilon(\vec{k}) = & -2t(\cos k_x + \cos k_y) \\ & - 96Wn_3(\cos k_x \pm \cos k_y), \end{aligned} \quad (\text{A20})$$

$$\begin{aligned} \Delta(\vec{k}) = & +Us_1 \\ & - 8Ws_1(\cos k_x \pm \cos k_y)^2 \\ & - 32Ws_2(\cos k_x \pm \cos k_y) \\ & - 32Ws_3. \end{aligned} \quad (\text{A21})$$

The energy constant \tilde{E}_{tUW}^{MF} stands for:

$$\tilde{E}_{tUW}^{MF} = -UNs_1^2 + 64WN(s_1s_3 + s_2^2 - \frac{1}{16}) + 192WNn_3^2. \quad (\text{A22})$$

Eq. (A19) can be diagonalized with a Bogoliubov – de Gennes transformation, similar to Eq. (A8), i. e.

$$\begin{pmatrix} \gamma_k^c \\ \gamma_k^v \end{pmatrix} = \begin{pmatrix} u(\vec{k}) & v(\vec{k}) \\ v(\vec{k}) & -u(\vec{k}) \end{pmatrix} \begin{pmatrix} \tilde{c}_{\vec{k},\uparrow} \\ \tilde{c}_{-\vec{k},\downarrow}^\dagger \end{pmatrix}, \quad (\text{A23})$$

$$u(\vec{k}) = \left[\frac{1}{2} \left(1 + \frac{\varepsilon(\vec{k})}{E(\vec{k})} \right) \right]^{\frac{1}{2}}, \quad (\text{A24})$$

$$v(\vec{k}) = \left[\frac{1}{2} \left(1 - \frac{\varepsilon(\vec{k})}{E(\vec{k})} \right) \right]^{\frac{1}{2}} \text{sign}(\Delta(\vec{k})). \quad (\text{A25})$$

The resulting Hamiltonian now becomes

$$\mathcal{H}_{tUW}^{MF} = \sum_{\vec{k}} E(\vec{k}) (\gamma_{\vec{k}}^{c\dagger} \gamma_{\vec{k}}^c - \gamma_{\vec{k}}^{v\dagger} \gamma_{\vec{k}}^v) + \tilde{E}_{tUW}^{MF}, \quad (\text{A26})$$

with the usual relation (Eq. (A11)) for $E(\vec{k})$.

The paramagnetic solutions can be easily obtained by setting the antiferromagnetic parameters in Eq. (A4), or the superconducting parameters in Eq. (A19), equal to zero.

APPENDIX B: DETAILS OF THE RPA CALCULATIONS

The W -dependent part V^W of the interaction vertex $\bar{\Gamma}^0$ is given by

$$\begin{aligned} V^W(\vec{k}, \vec{k}', \vec{q}) = & -8W[(\cos k'_x \pm \cos k'_y)(\cos k_x \pm \cos k_y) \\ & + (\cos(k'_x - q_x) \pm \cos(k'_y - q_y))(\cos k_x \pm \cos k_y) \\ & + (\cos(k_x + q_x) \pm \cos(k_y + q_y))(\cos k'_x \pm \cos k'_y) \\ & + (\cos(k_x + q_x) \pm \cos(k_y + q_y))(\cos(k'_x - q_x) \pm \cos(k'_y - q_y))]. \end{aligned} \quad (\text{B1})$$

¹ M. G. Zacher, W. Hanke, E. Arrigoni, and S.-C. Zhang, cond-mat/9912161; S.-C. Zhang, J.-P. Hu, E. Arrigoni, W. Hanke and A. Auerbach, Phys. Rev. B **60**, 13070 (1999).

² S. Murakami and N. Nagaosa, cond-mat/9910001.

³ E. Arrigoni and W. Hanke, Phys. Rev. Lett. **82**, 2115 (1999).

⁴ S.-C. Zhang, Science **275**, 1089 (1997).

⁵ W. P. Wu, J. R. Schrieffer and A. J. Heeger, Phys. Rev. B **22**, 2099 (1980)

⁶ F. F. Assaad, M. Imada and D. J. Scalapino, Phys. Rev. Lett. **77**, 4592 (1996)

⁷ F. F. Assaad, M. Imada and D. J. Scalapino, Phys. Rev. B **56**, 15001 (1997)

⁸ F. F. Assaad, condmat/9806306 (1998)

⁹ F. F. Assaad and M. Imada, Phys. Rev. B **58**, 1845 (1998)

¹⁰ F. F. Assaad and M. Imada, condmat/9811384 (1998)

¹¹ F. F. Assaad, *unpublished* (1999)

¹² J. R. Schrieffer, X. G. Wen and S.-C. Zhang, Phys. Rev. B **39**, 11663 (1989)

¹³ D. M. Frenkel and W. Hanke, Phys. Rev. B **42**, 6711 (1990)

¹⁴ see, for example, W.-G. Yin, C.-D. Gong and P. W. Leung, Phys. Rev. Lett. **81**, 2534 (1998), and D. Duffy and A. Moreo, Phys. Rev. B **52**, 15607 (1995)

¹⁵ M. G. Zacher, *Dissertation* (1999)

¹⁶ A. L. Fetter and J. D. Walecka, *Quantum Theory of Many-Particle Systems* (1971)

¹⁷ W. Hanke and L. J. Sham Phys. Rev. B **12**, 4501 (1975)

\vec{r}	$P_s^v(\vec{r})$	$P_d^v(\vec{r})$
(0, 0)	0.2950 ± 0.0018	0.1304 ± 0.0011
(0, 1)	0.0932 ± 0.0009	0.0238 ± 0.0006
(0, 2)	0.0076 ± 0.0002	0.0252 ± 0.0003

TABLE I. Short range vertex contribution of pair-field correlations in the extended s - and d -wave channels for the pure $t - U - W$ model, obtained from QMC simulations. Here we consider an $L = 24$ lattice at $W/t = 0.35$, $U/t = 2$ and $\langle n \rangle = 1$. We choose antiperiodic (periodic) boundary conditions in the x (y) direction. The distance \vec{r} is in units of the lattice constant.

\vec{r}	$P_s^v(\vec{r})$	$P_d^v(\vec{r})$
(0, 0)	1.661 ± 0.079	3.082 ± 0.066
(0, 1)	0.373 ± 0.020	1.107 ± 0.015
(0, 2)	0.091 ± 0.008	0.119 ± 0.004

TABLE II. Short range vertex contribution of pair-field correlations in the extended s - and d -wave channels for the $t - U - W$ model with phase factors, obtained from QMC simulations. Here we consider an $L = 10$ lattice at $W/t = 0.35$, $U/t = 4$ and $\langle n \rangle = 1$. We choose periodic boundary conditions. The distance \vec{r} is in units of the lattice constant.

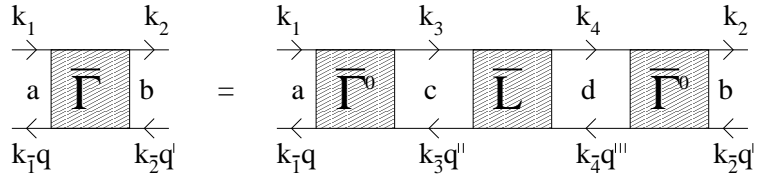


FIG. 1. Diagrammatic representation of the fluctuation vertex

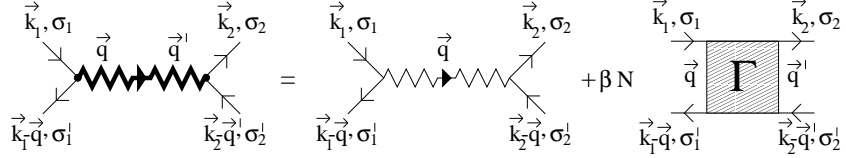


FIG. 2. Diagrammatic representation of the effective interaction

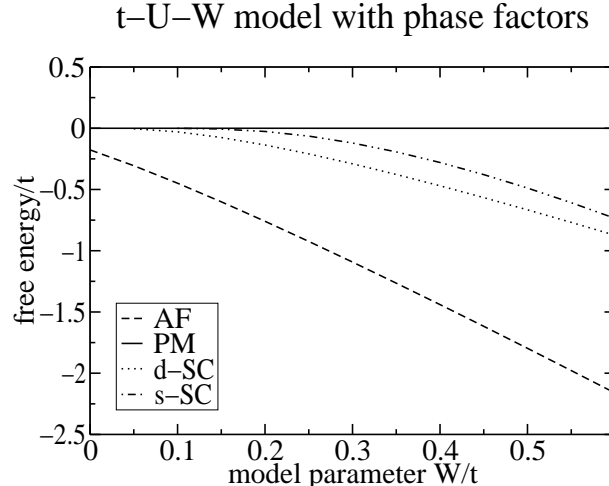
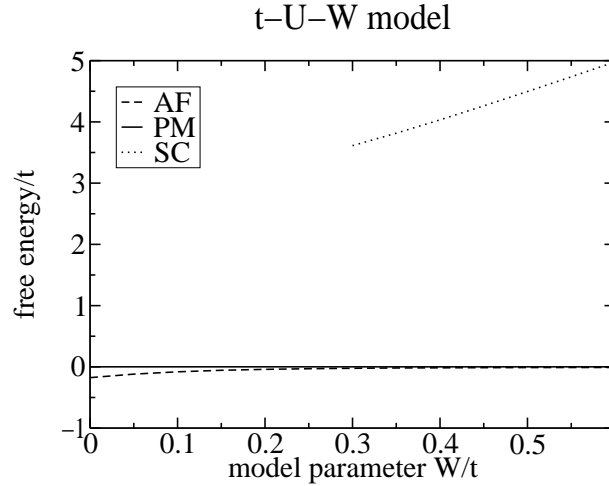


FIG. 3. Free energy per lattice site of the different phases of the pure $t - U - W$ model (top) and the $t - U - W$ model with phase factors (bottom). Plotted is the difference to the paramagnetic energy ($U = 4t$, $T = 0K$, $\mu = 0t$, lattice size: 60×60).

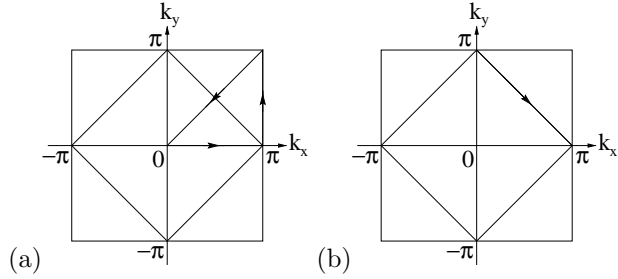


FIG. 4. Paths followed through the Brillouin zone to plot the energy bands of Fig. 5.

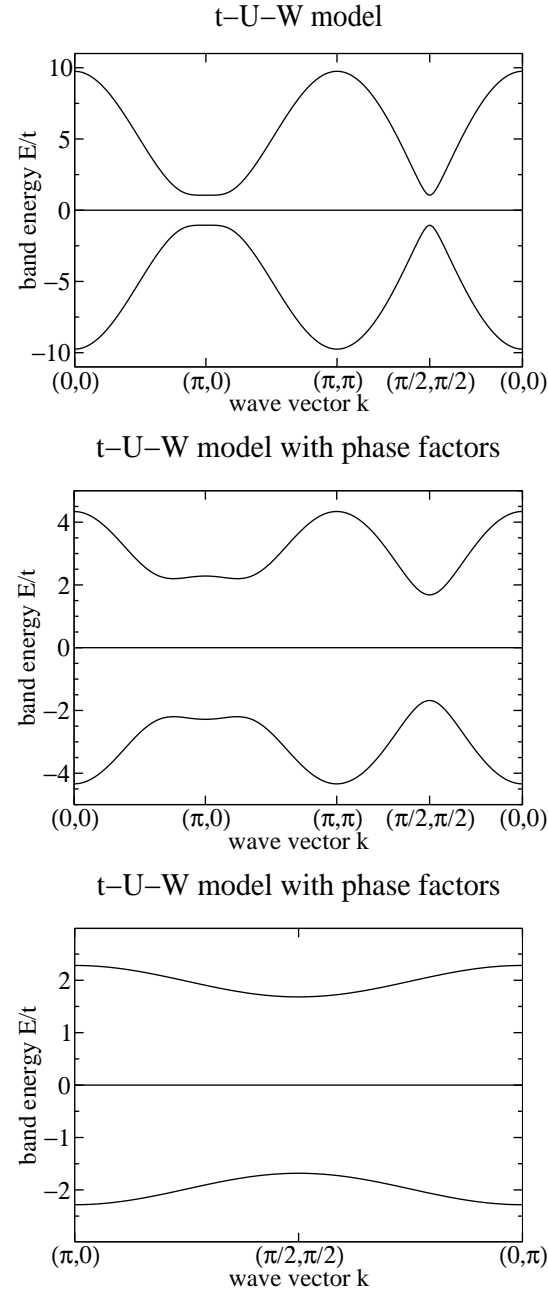


FIG. 5. Energy bands of the pure $t - U - W$ model (upper graph, $W = 0.15t$) and of the $t - U - W$ model with phase factors (middle and lower graph, $W = 0.05t$) on the paths shown in Figs. 4(a), for upper and middle graph, and 4(b) for lower graph ($U = 4t$, $T = 0K$, $\mu = 0t$, lattice size: 100×100).

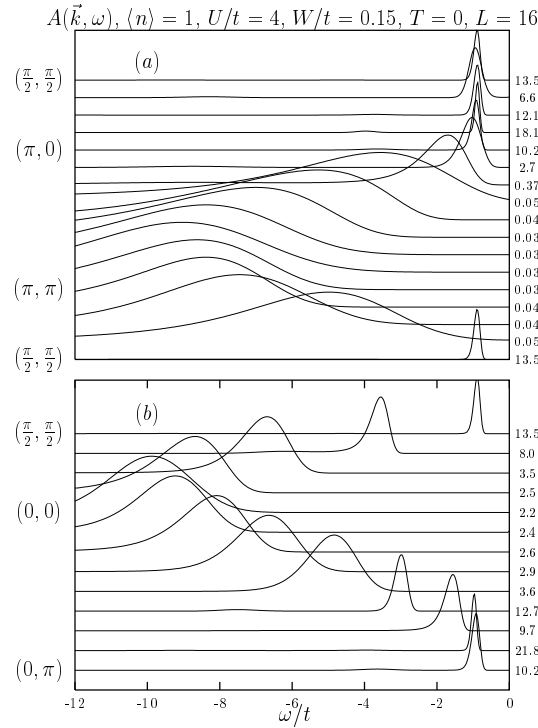


FIG. 6. Spectral weight $A(\vec{k}, \omega)$ of the pure $t - U - W$ model, obtained from QMC simulations ($U = 4t$, $W = 0.15t$, $T = 0K$, $\mu = 0t$) (from 10). The considered path in the Brillouin zone is listed on the left hand side of the figure. We have normalized the raw data by the factor listed on the right hand side of the figure. This normalization sets the peak value of $A(\vec{k}, \omega)$ to unity for all considered \vec{k} vectors.

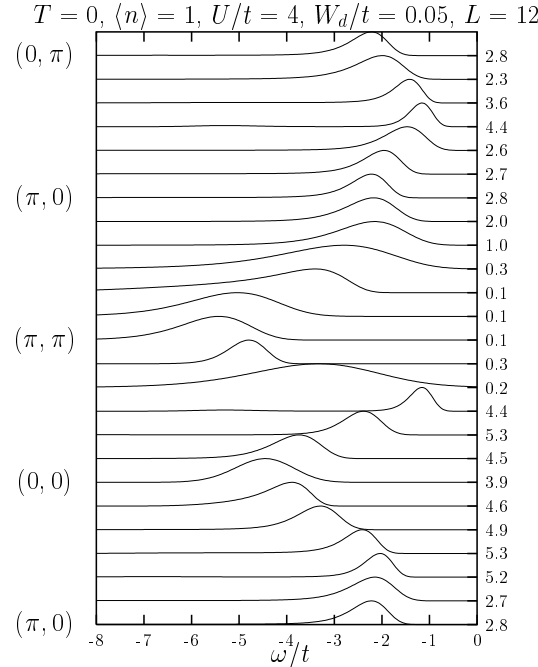


FIG. 7. Spectral weight $A(\vec{k}, \omega)$ of the $t - U - W$ model with phase factors, obtained from QMC simulations ($U = 4t$, $W = 0.05t$, $T = 0K$, $\mu = 0t$) (from 11).

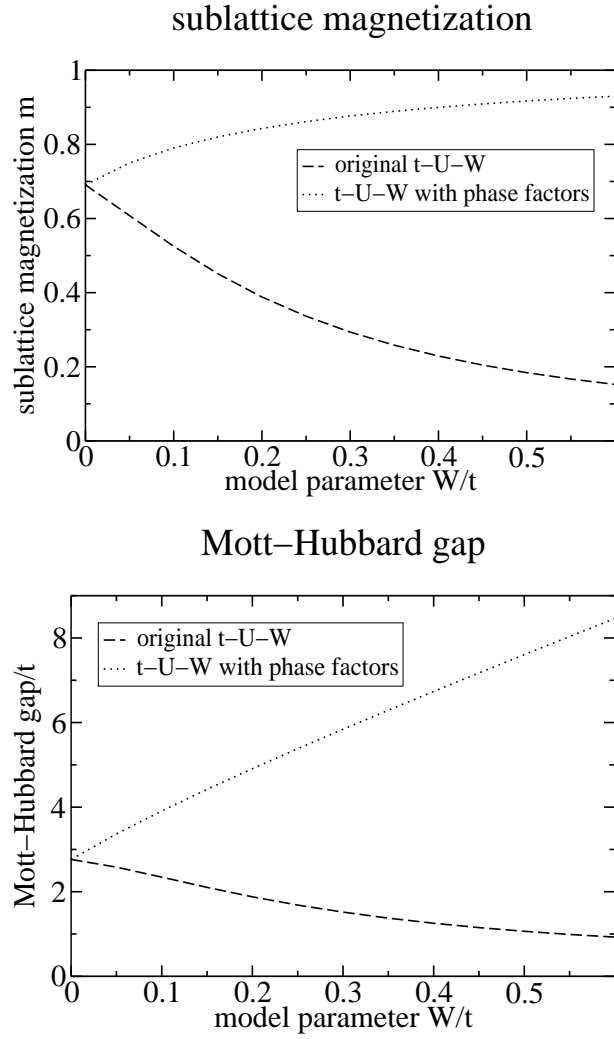


FIG. 8. Sublattice magnetization (top) and Mott-Hubbard gap (bottom) of the $t - U - W$ model as a function of W ($U = 4t$, $T = 0K$, $\mu = 0t$, lattice size: 100×100).

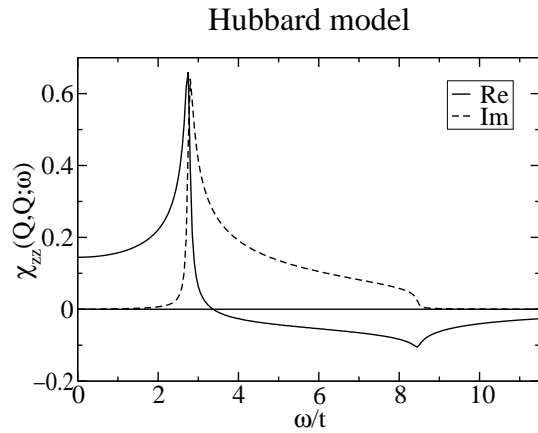
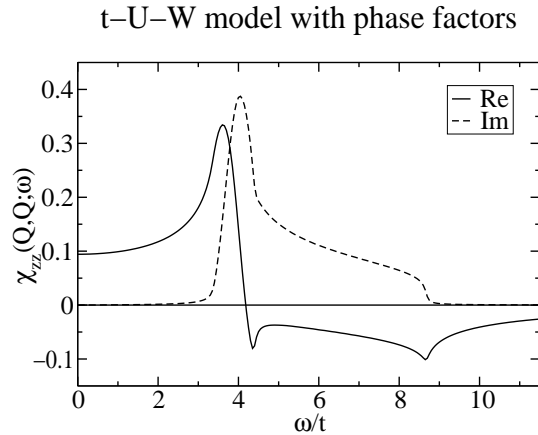
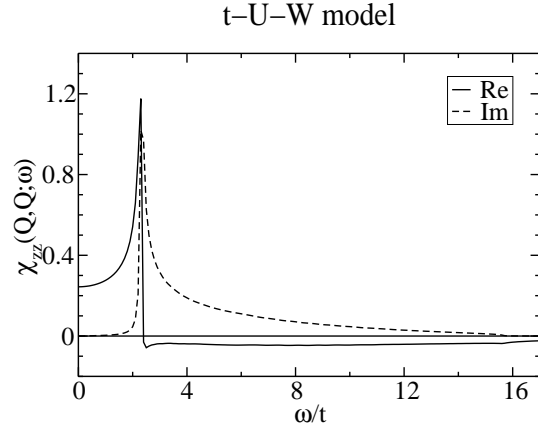
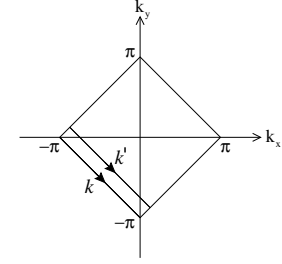
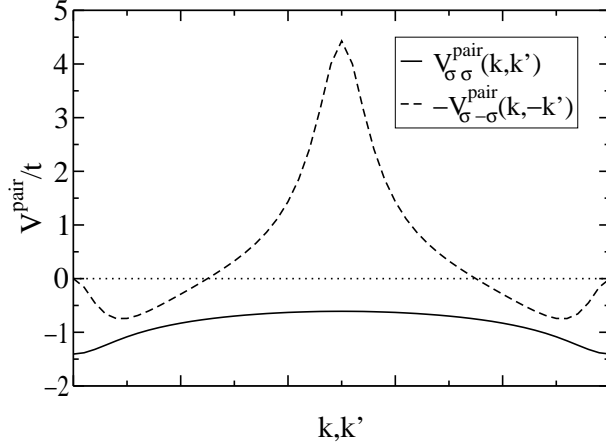


FIG. 9. Longitudinal spin susceptibility $\chi_{zz}(\vec{Q}, \vec{Q}; \omega)$ of the pure $t - U - W$ model (top, $W = 0.1t$), the $t - U - W$ model with phase factors (middle, $W = 0.05t$) and the Hubbard model (bottom, $W = 0t$); (as usual: $U = 4t$, $T = 0K$, $\mu = 0t$).



t-U-W model



Hubbard model

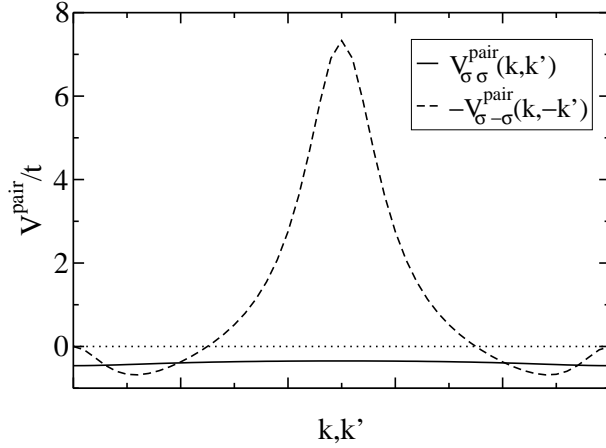
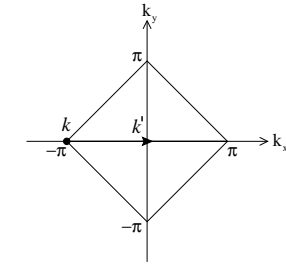
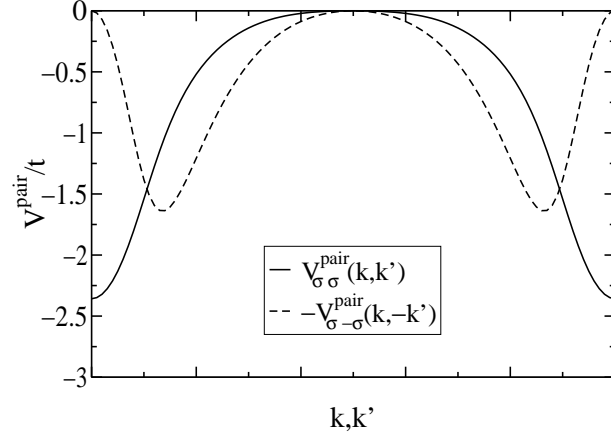


FIG. 10. Direct part $V_{\sigma\sigma}^{\text{pair}}(\vec{k}, \vec{k}')$ and exchange part $-V_{\sigma-\sigma}^{\text{pair}}(\vec{k}, -\vec{k}')$ of the pairing-potential for the pure $t - U - W$ model (top, $W = 0.1t$) and for the Hubbard model (bottom, $W = 0t$). The paths shown above were followed by \vec{k} and \vec{k}' through the MBZ. The distance between \vec{k} and \vec{k}' amounts $\vec{\delta k} \approx 0.14\pi$ ($U = 4t$, $T = 0K$, $\mu = 0t$, lattice size: 100×100).



t-U-W model



Hubbard model

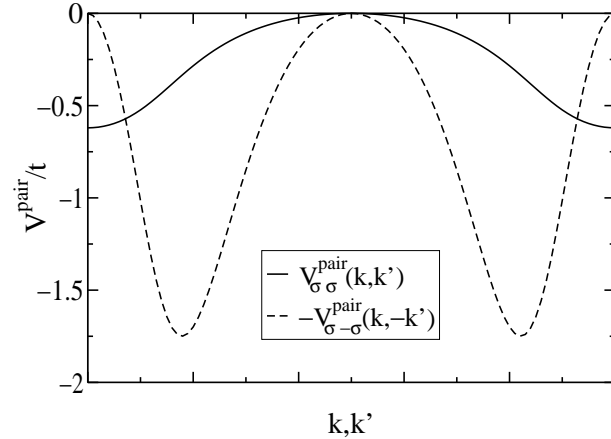
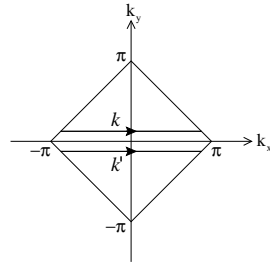
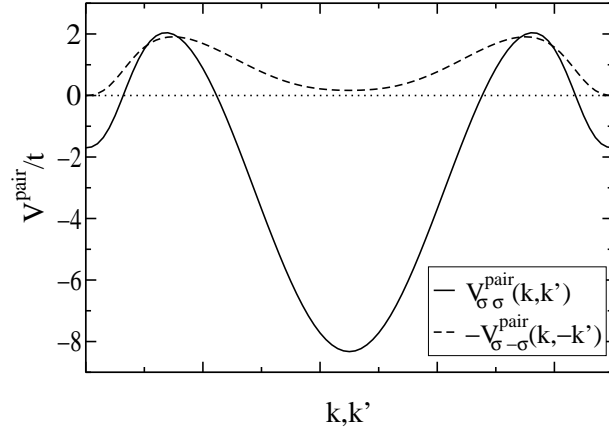


FIG. 11. Direct part $V_{\sigma\sigma}^{\text{pair}}(\vec{k}, \vec{k}')$ and exchange part $-V_{\sigma-\sigma}^{\text{pair}}(\vec{k}, -\vec{k}')$ of the pairing-potential for the pure $t - U - W$ model (top, $W = 0.1t$) and for the Hubbard model (bottom, $W = 0t$). The path shown above was followed by \vec{k}' through the MBZ with \vec{k} held constant ($U = 4t$, $T = 0K$, $\mu = 0t$, lattice size: 100×100).



t-U-W model



Hubbard model

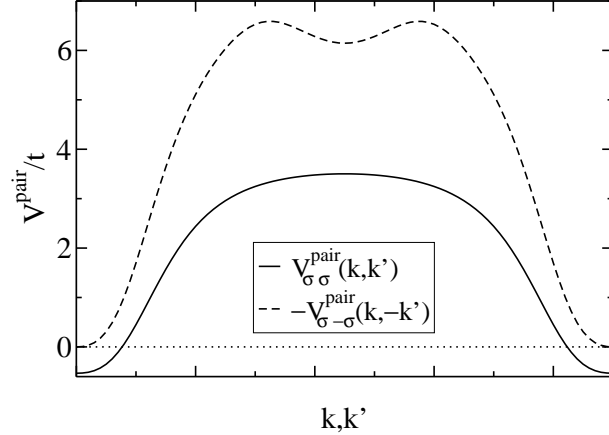


FIG. 12. Direct part $V_{\sigma\sigma}^{\text{pair}}(\vec{k}, \vec{k}')$ and exchange part $-V_{\sigma-\sigma}^{\text{pair}}(\vec{k}, -\vec{k}')$ of the pairing-potential for the pure $t - U - W$ model (top, $W = 0.1t$) and for the Hubbard model (bottom, $W = 0t$) The paths shown above were followed by \vec{k} and \vec{k}' through the MBZ. The distance between \vec{k} and \vec{k}' amounts $\delta\vec{k} \approx 0.2\pi$ ($U = 4t$, $T = 0K$, $\mu = 0t$, lattice size: 100×100).

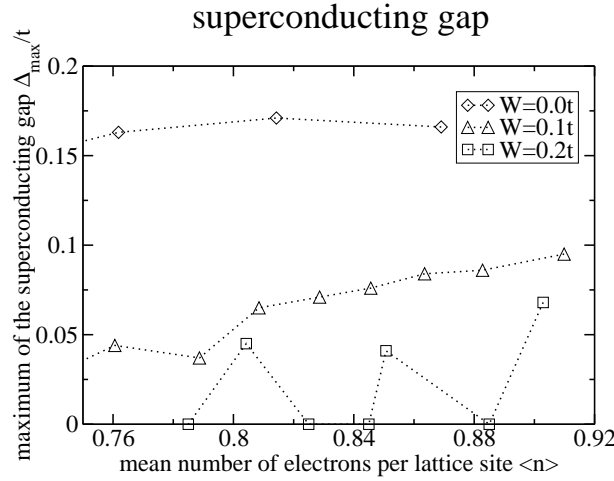


FIG. 13. Maximum value of the superconducting gap function $\Delta_{max} = \max \Delta(\vec{k})$ as a function of the mean electron number per lattice site $\langle n \rangle$ for different values of the model parameter W ($U = 4t$, $T = 0K$, lattice size: 20×20 , d -wave symmetry).

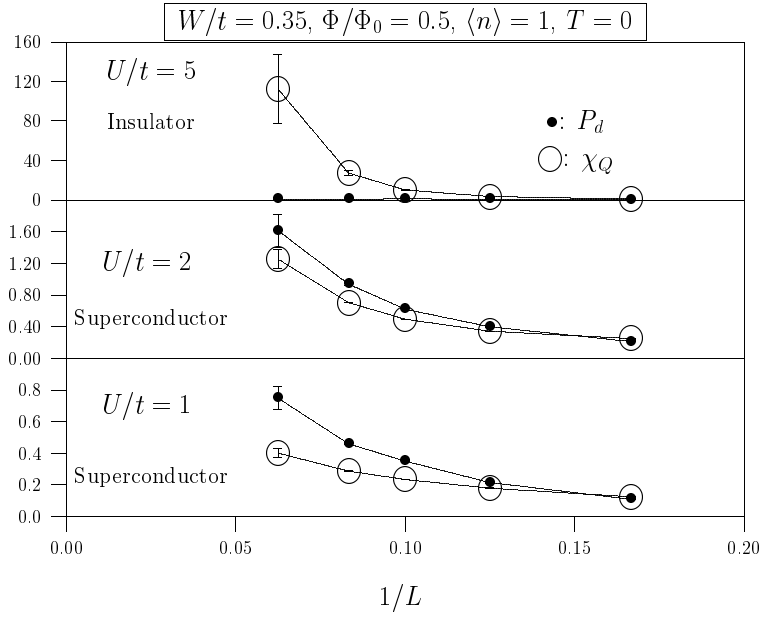


FIG. 14. Vertex contribution to the d -wave pairing correlations (\bullet) and staggered spin susceptibility (\circ) for the pure $t - U - W$ model, obtained from QMC simulations.